Selected aspects of the classical molecular dynamics of *N* particles in strong interaction

D. Cussol
LPC, Caen (IN2P3-CNRS/ISMRA et Université), F-14050 Caen Cedex, France
(Received 27 November 2001; published 9 May 2002)

Selected results of a classical simulation of *N* particles in strong interaction are presented. The static properties of such classical systems are qualitatively similar to the known properties of atomic nuclei. The simulations of collisions show that all observed reaction mechanisms in nucleus-nucleus collisions are present in this numerical simulation. The first studies of such collisions are in qualitative agreement with experimental observations. This simulation could shed new light on energy deposition in heavy ion collisions: the excitation energy of each cluster is found to be lower than the energy of the least bound particle in the cluster. Finally, the similarities of fragmentation pattern with those obtained with a statistical code indicate that an unambiguous link can be established between the statistical and the dynamical descriptions of reaction mechanisms.

DOI: 10.1103/PhysRevC.65.054614 PACS number(s): 24.10.Cn, 25.70.−z

Over the last decades, heavy ion collisions have been widely used and intensively studied experimentally to determine the equation of state of nuclear matter. Many reaction mechanisms have been identified and a lot of theoretical works have been induced. Schematically, the incident energy domain has been divided in three parts: the low energy range, up to 10–20 *A* MeV, where fusion and deep inelastic processes are dominant; the high energy range, above 100*A* MeV, where the nucleonic and subnucleonic degrees of freedom start to play a significant role; and the intermediate energy range, from 20*A* MeV to 100*A* MeV, where binary processes and multifragmentation take place. At each energy range, the reaction is schematically described as a two-step process: an entrance channel during which the excited nuclei are formed, and a decay stage where the excited fragments cool down by particle or fragment emissions.

Theoretically, the entrance channel of the reaction is mainly described by dynamical models. At low energy, the attractive character of the interaction is dominant and the entrance channel is described mainly by mean-field approaches [1]. At high energies, the repulsive part of the interaction and its nucleon-nucleon character are dominant and cascade models are mainly used to describe the first moments of the collision [2]. At intermediate energies, the attractive part and the repulsive part of the interaction interfere. Transport models are widely used to describe the entrance channel at this energy range [3–9]. They contain a mean-field part through the one-body evolution of the system, and a nucleon-nucleon part through the collision term. At all energy ranges, the decay stage is mainly described by statistical decay models (GEMINI [10], SIMON [11], SMM [12], MMMC [13], QSM [14], EES [15], etc.) which assume that the nuclei formed during the first dynamical step are equilibrated.

With this scheme, it is very hard to have a global and consistent description of nucleus-nucleus collisions. Although the nucleon-nucleon interaction is the same, whatever the incident energy and whatever the reaction time, different models are used depending on the energy range and the reaction time. The links between these different models are not obvious. For example, how can the liquid-drop parametrization used in the statistical decay code be deduced from the parameters of the interaction used in a transport code? What is the link between the incompressibility modulus of nuclear matter K_∞ and the nucleon-nucleon cross section σ_{nn}? Is the statistical description still justified when the thermalization time is close to or longer than the lifetime of excited nuclei?

The present status results mainly from the impossibility to solve the full nuclear many-body problem. To solve it, approximations are made, depending on the energy range and on the reaction time. Even after simplifications, the resulting equations do not have analytical solutions and they are often solved numerically. It seems hard nowadays to connect these different models to have a global description of the processes involved in nucleus-nucleus collisions.

Nevertheless, some attempts were made to describe globally nucleus-nucleus reactions at intermediate energies by using (semi)classical molecular dynamics codes [16–22]. The main advantage of these codes is that the classical many-body problem can be solved numerically with a high accuracy without any assumption. The main drawback is that the quantum character of the system is ignored. A lot of work has already been done with the help of such codes to study the mechanism of fragment formation in multifragmentation. Could these codes do better by describing the whole reaction process, from the very beginning of the reaction up to the decay stage? Are they able to make a link between the different energy ranges? Which processes are accessible with the simplest hypotheses?

This paper will show that classical molecular dynamics simulations are interesting tools to establish the links between the different approaches used in nucleus-nucleus collisions. There will be no attempt to reproduce experimental data of nucleus-nucleus collisions since essential physical ingredients are missing in the presented simulation. The purpose of this paper is to see what can be obtained with the simplest hypotheses. To have a quantitative reproduction, the quantum effects, the Coulomb interaction, and a momentum dependent interaction should be added. There are, of course, essential differences between quantum and classical systems (see, for example, [23]). These differences will not be addressed in this paper, since its main aim is to see what can be obtained with the simplest simulation. In the first section, the classical *N*-body dynamics code will be briefly described. The static properties of stable *n*-body systems will be studied in Sec. II. Some examples of reaction mechanisms and some

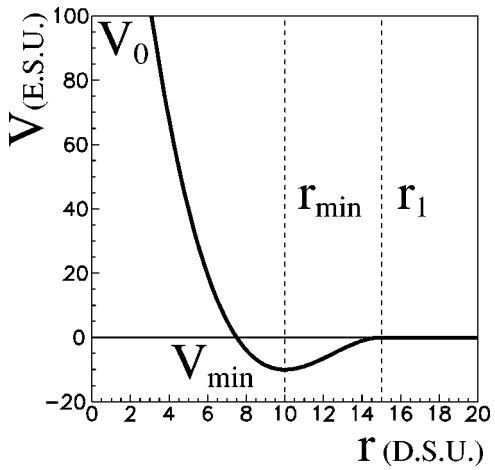

FIG. 1. Shape of the interaction used in the CNBD simulation.

analyses of cluster-cluster collisions are given in Sec. III. Finally, conclusions will be drawn.

I. DESCRIPTION OF THE CODE

Let us start by describing the classical N-body dynamics code (labeled CNBD) used in this paper. The basic ingredients of such a code are very simple. The system consists of N identical pointlike particles in mutual interaction. The dynamical evolution of each particle of the system is driven by the classical Newtonian equations of motion. The two-body potential used in the present work is a third degree polynomial. The depth value is V_{min} and the value at $r=0$ is finite and equal to V_0. It reads

$$V(r)=\begin{cases} V_0+ar+br^2+cr^3 & \text{if } r\leqslant r_1 \\ 0 & \text{if } r>r_1, \end{cases} \tag{1}$$

where the parameters a, b, and c are determined such that $V(r_{min})=V_{min}$ and that $\partial V(r)/\partial r$ is null for $r=r_{min}$ and for $r=r_1$. The shape of the two-body potential is shown in Fig. 1. This potential has the basic properties of the Lennard-Jones potential used in other works [21,22]: a finite range attractive part and a repulsive short range part. To follow the dynamical evolution of the system an adaptative step size fourth-order Runge-Kutta algorithm is used [24]. The main difference with other works is that the time step Δt can vary: if the potential varies strongly, Δt is small and when the potential varies gently, Δt becomes larger. This allows a very high accuracy with shorter CPU time than for fixed time step algorithms. It requires an additional simulation accuracy parameter ϵ, which is adjusted to ensure the verification of conservation laws (energy, momentum, angular momentum) with a reasonable simulation time. For an ϵ value of 10^{-5}, typical CPU times for a collision of two clusters each with 50 particles and for a total time equal to 200 time simulations units on a Compaq DS20 computer under the UNIX TRUE64 operating system ranges from ≈ 30 to ≈ 400 s, depending mainly on the impact parameter. The total energy difference between the initial and the the final times is lower than 0.001%. This simulation has five free parameters: four linked to the physics (the interaction) and one linked to the numerical algorithm (ϵ).

Since one wants to study the simplest case, neither long range repulsive interaction nor quantum corrections like a Pauli potential have been introduced [25]. Additionally, no statistical decay code is applied on the excited fragments formed during the collision. The final products have to be regarded as ''primary'' products that will decay afterwards.

In order to avoid any confusion with nuclear physics, the units used here are arbitrary. The distances will then be in distance simulation units (DSU), the energies in energy simulation units (ESU), the time in time simulation units (TSU) and the velocities in DSU/TSU. We will only be interested in the relative evolutions of the observables and in their link to the properties of the stable systems. The main goal of the present work is not to reproduce the experimental data of nucleus-nucleus collisions, but rather to see to what extent this simple simulation is qualitatively similar, or not, to experimental data.

II. STATIC PROPERTIES OF "GROUND STATES"

Once the basic ingredients are defined, one can build stable systems. Since the two-body potential only depends on the distance between the two particles, such systems are small crystals. The ground states of such systems are defined as the configuration in position space that minimizes their total energy. This is obtained by using a Metropolis simulated annealing method [24]. The locations of particles obtained in this way are very close to those obtained by using a basin-hopping algorithm for Lennard-Jones clusters [26].

In the upper left panel of Fig. 2 is displayed the energy per particle E_{Bind}/N of these ground states as a function of the number N of particles in the cluster (solid line). The dashed and dotted line corresponds to a fit using a liquid-drop formula. The dashed line corresponds to the energy of the least bound particle $E_{LeastBound}$ in the cluster. This energy is defined as follows:

$$E_{LeastBound}=\max_{j=1,N}\left[\sum_{i\neq j} V(r_{ij})\right], \tag{2}$$

where r_{ij} is the relative distance between the particles i and j and $V(r_{ij})$ is the value of the two-body potential. It will be seen that $E_{LeastBound}$ seems to play a particular role in the simulated cluster-cluster collisions. The overall dependence of E_{Bind}/N with N is very similar to what is seen in nuclear physics. The main difference is seen for high values of N because of the absence of a Coulomb-like interaction: E_{Bind}/N continues to decrease with N whereas it increases for nuclei. These values are close to those found by using the basin-hopping algorithm [26].

The dependence with N of the root mean square radius $r(N)=\sqrt{<r^2>}$ of N-body clusters is shown on the upper right panel of Fig. 2 (solid line). The dashed and dotted line corresponds to a fit using a $N^{1/3}$ term. Here again, this is similar to what is known for nuclei. The main difference is

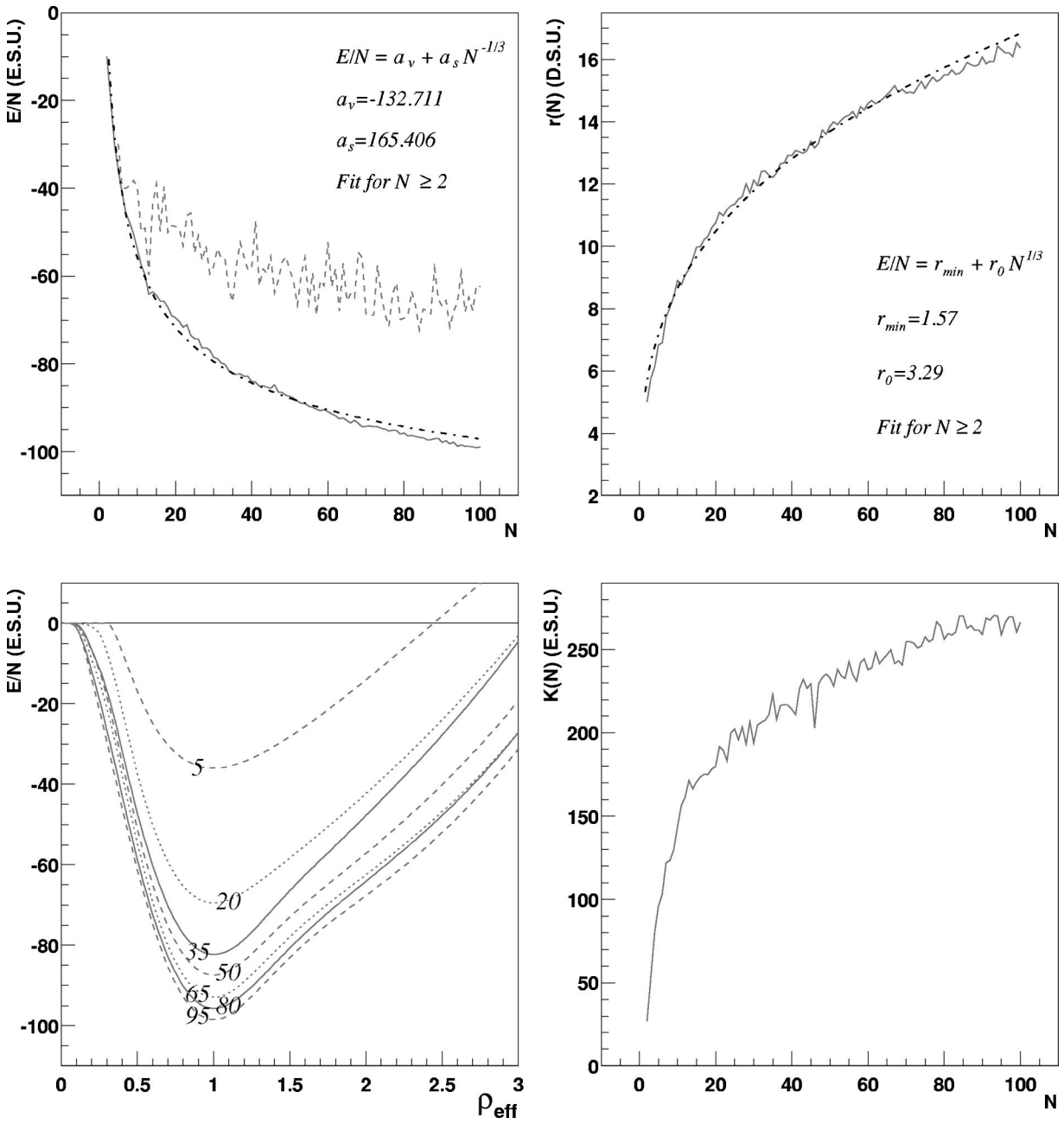

FIG. 2. Energy per particle (upper left panel) and root mean square radius (upper right panel) of N-body clusters as functions of N. For these two panels, the full lines correspond to the obtained values and the dashed and dotted lines to a fit. On the left panel, the dashed line corresponds to the energy of the least bound particle in the cluster. Lower row: zero temperature equation of state for different $N=5$, $N=20$, $N=35$, $N=50$, $N=65$, $N=80$, and $N=90$ (left) and incompressibility modulus $K(N)$ as a function of N (right).

the r_{min} term, which is due to the large size of the repulsive core compared to the range of the attractive part of the interaction.

Since a size can be defined, an effective density can be calculated. One can stretch and squeeze the N-body cluster and build an effective zero temperature equation of state. This is displayed on the lower left panel of Fig. 2 for various system sizes. The density ρ_{eff} on this abscissa is the density relative to the density for the ground state. The curvature of this equation of state at ground state density can be computed and defined as the compressibility modulus $K(N)$ $=[\partial^2(E/N)/\partial\rho_{eff}^2]_{\rho_{eff}=1}$ of the system. Its variations with N are displayed on the lower right panel of Fig. 2. One can see on these two plots that the ''equation of state'' and $K(N)$ are strongly dependent on N for values of N below 20–30 and then less dependent on N for larger systems. One could, in principle, define an equation of state of infinite matter by computing the asymptotic limits of these evolutions for very large values of N.

This first study shows that static properties of the classical N-body clusters have strong similarities with those of atomic nuclei. This suggests that all the parametrization used to de-

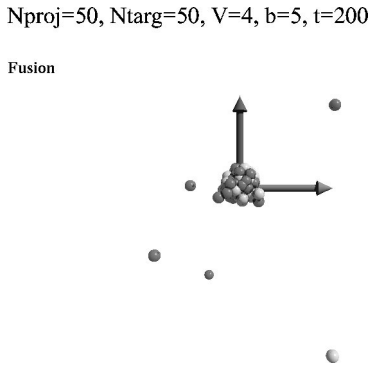

FIG. 3. Fusion reaction.

scribe these systems (liquid-drop parametrization, radii, equation of state, etc.) could be directly deduced from the parameters of the two-body interaction. Since the interaction remains unchanged whatever the cluster, the differences seen for different cluster sizes have to be attributed only to the number of particles N and to the geometrical configuration of the particles in the clusters.

III. CLUSTER-CLUSTER COLLISIONS

After studying the static properties of stable N-body systems, collisions between clusters can be investigated to see what kind of reaction can be obtained. Roughly 20 000 collisions have been generated for different system sizes, different entrance channel asymmetries, and different impact parameters. For each collision, the orientation of the inertia axis of clusters are randomly chosen. This avoids performing the same collision twice if the impact parameter, target and projectile size, and the incident energy are the same for two different collisions. The simulations have been performed for the following systems: $13+13$, $34+34$, $50+50$, $100+100$, and $18+50$. The incident energies have been chosen in such a way that the available energy in the center of mass frame ranges from an energy far below the binding energy of the fused system (≈ 30 ESU) to an energy well above the binding energy of the fused system (≈ 120 ESU). As it will be shown, these collisions can be studied in the same way as the experimental data of nucleus-nucleus collisions. These collisions can be seen as numerical experiments. Only few examples of such analyses will be shown. More detailed analyses will be made in forthcoming papers. First, a small list of reaction mechanisms obtained will be given. Second, the excitation energy stored in excited clusters will be studied and a link to the static properties will be made. Finally,

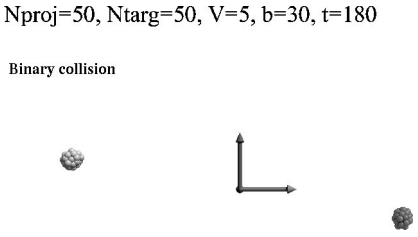

FIG. 4. Binary reaction.

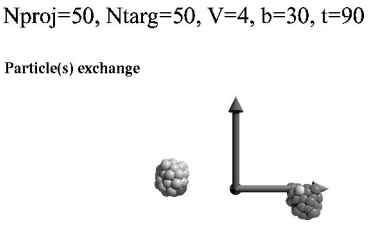

FIG. 5. Particles exchange reaction. The particle captured by the projectile is in light gray in the top of dark gray system. The particle captured by the target is in dark gray in the bottom of light gray system.

the question of the statistical description of this dynamical model will be briefly addressed.

A. Reaction mechanisms

Figures 3–9 display pictures of cluster-cluster collisions in the center of mass frame obtained after a fixed time. In each picture, the particles that were originally belonging to the projectile are in dark gray and those that were belonging to the target are in light gray. The projectile velocity V is in DSU/TSU, the impact parameter b in DSU and the time t in TSU. The horizontal arrow corresponds to the projectile velocity direction. The vertical arrow corresponds to the direction perpendicular to the projectile velocity in the reaction plane. The most striking observation is that all kinds of reaction mechanisms observed in nucleus-nucleus collisions seem to be present in this very simple simulation. One can see low energy processes such as the fusion/evaporation process (Fig. 3), pure binary collision (Fig. 4), stripping/pickup mechanism (Fig. 5), and deep inelastic collisions (Fig. 6). Intermediate energy processes, like neck formation and breakup (Fig. 7) and multifragmentation (Fig. 8), are seen. Finally, high energy processes like the participant/spectator process (Fig. 9) are also seen.

This similarity can also be seen on the so-called Wilczynski plots [27] shown in Fig. 10. These plots display the correlation between the flow angle θ_{flow} and the total kinetic energy of the clusters $E_{kin}=\Sigma_i E^i_{kin}$ where E^i_{kin} is the kinetic energy of cluster i in the center of mass frame. θ_{flow} is the angle of the main axis of the event relative to the projectile velocity direction. This axis is the principal axis of the kinetic energy tensor $T_{ij}=\Sigma_k P^i_k P^j_k/N_k$, where P^i_k, $i=x,y,z$ are the coordinates of the momentum in the center of mass

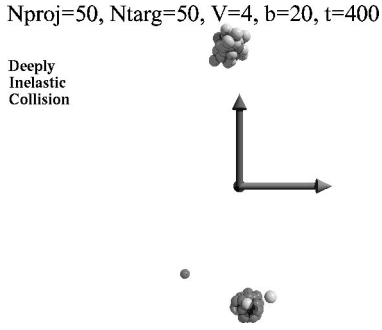

FIG. 6. Deeply inelastic collision.

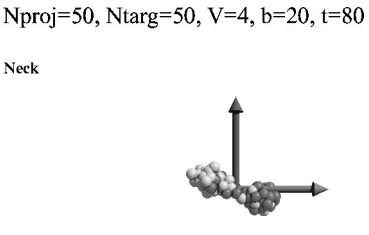

FIG. 7. Neck formation.

frame of cluster k and N_k its number of particles. Two particles are assumed to belong to the same cluster if they are in interaction, i.e., if their relative distance is below the range r_1 of the interaction (see Fig. 1). This algorithm of cluster recognition is the simplest one and is called minimum spanning tree algorithm in other works [22,28]. The most dissipative collisions correspond to the smallest E_{kin} values: the available energy is converted into internal energy of clusters. These plots were built for a $N=34$ projectile colliding a $N=34$ target at four available energies $E_{\mathrm{c.m.}}/N$ in the center of mass, where $N=N_{proj}+N_{targ}$ is the total number of particles: $E_{\mathrm{c.m.}}/N=60$ ESU, $E_{\mathrm{c.m.}}/N=90$ ESU, $E_{\mathrm{c.m.}}/N=120$ ESU and $E_{\mathrm{c.m.}}/N=30$ ESU, which correspond respectively, to the energy of the least bound particle for the fused $N=68$, cluster, to the binding energy per particle for $N=68$, to the energy of the most bound particle for $N=68$, and to an energy below the energy of the least bound particle for $N=68$. The relative velocity v_{rel} between the projectile and the target is determined such that $E_{\mathrm{c.m.}}/N$ corresponds to the desired value:

$$v_{rel}=\sqrt{\frac{2E_{\mathrm{c.m.}}(N_{proj}+N_{targ})}{m_p N_{proj} N_{targ}}}, \tag{3}$$

where m_p is the mass of a particle. Its value has been arbitrarily fixed to 20 mass simulation units. For each energy, 1 000 collisions have been computed assuming a flat impact parameter distribution ranging from $b=0$ DSU to the sum of the two cluster radii plus the range of the interaction $b_{max}=r(N_{proj})+r(N_{targ})+r_1$, where r_1 is the range of the two-body interaction). In the analyses, each collision is weighted assuming a triangular impact parameter distribution between 0 and b_{max} (weight$\propto b$).

At $E_{\mathrm{c.m.}}/N=30$ ESU (upper left panel), the flow angle is always negative. This means that the projectile and the targetlike clusters are deflected to the opposite direction relative to their original one. At this energy, the attractive part of the interaction is dominant. For the lowest E_{kin} values, all possible values of θ_{flow} are covered: this corresponds to the fusion/evaporation process. At $E_{\mathrm{c.m.}}/N=60$ ESU (upper right panel), the picture is changed and the range of θ_{flow} values is smaller than for the previous energy: the repulsive part starts to act. The fusion/evaporation area (small E_{kin} values, all θ_{flow} values) is still present. For the two highest energies (lower panels), the picture is roughly the same. For the less dissipative collisions, the attractive part is still dominant (negative θ_{flow} values). But when the dissipation increases, the repulsive part becomes dominant and the projectile and the target bounce on each other (positive θ_{flow} values). For the most dissipative collisions, only positive θ_{flow} values are seen, which indicates the disappearance of the fusion/evaporation process. These evolutions are qualitatively similar to what is seen in nucleus-nucleus collisions (see, for example, [29]).

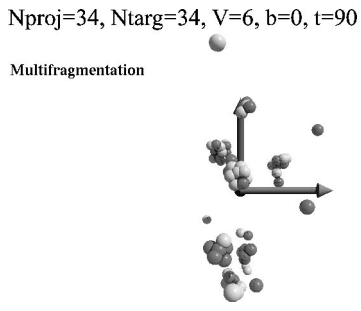

FIG. 8. Multifragmentation reaction.

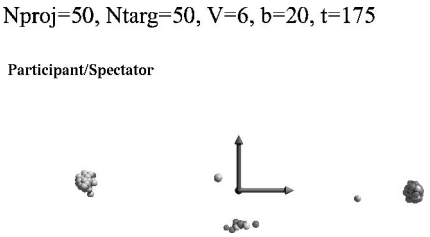

FIG. 9. Participant-spectator reaction.

These two studies indicate that the description of the reaction mechanisms in terms of the mean field at low energies and in terms of particle-particle collisions at high energies can be deduced from the properties of the two-body interaction alone. The similarities of this classical N-body simulation with mechanisms observed in nucleus-nucleus collisions suggest that, apart from quantum mechanical effects, an effective and unified description of nucleus-nucleus collisions could be obtained with a reduced number of parameters. Providing the interaction has a finite range attractive part and a short range repulsive part, the overall behavior of the N-body systems seems to be independent of the values of the parameters of this interaction. Of course, for a more quantitative agreement with nucleus-nucleus collisions, additional physical ingredients (quantum mechanics, Coulomb interaction, momentum dependent interaction) have to be included.

B. Energy deposition in clusters

Let us now focus our study of cluster-cluster collisions on selected topics. Of particular interest is the excitation energy stored in clusters. How can this energy be linked to the available energy and how is it linked to the properties of the ground-state characteristics of these clusters?

One can plot, for example, the correlation between the excitation energy E^*/N of the cluster and its parallel velocity $V_{\parallel}$ for $N_{proj}=34$ on $N_{targ}=34$ collisions (Fig. 11) for the whole impact parameter range. The excitation energy of each cluster is simply the difference between the total energy (potential plus kinetic) and the ground-state energy of the cluster. It reads

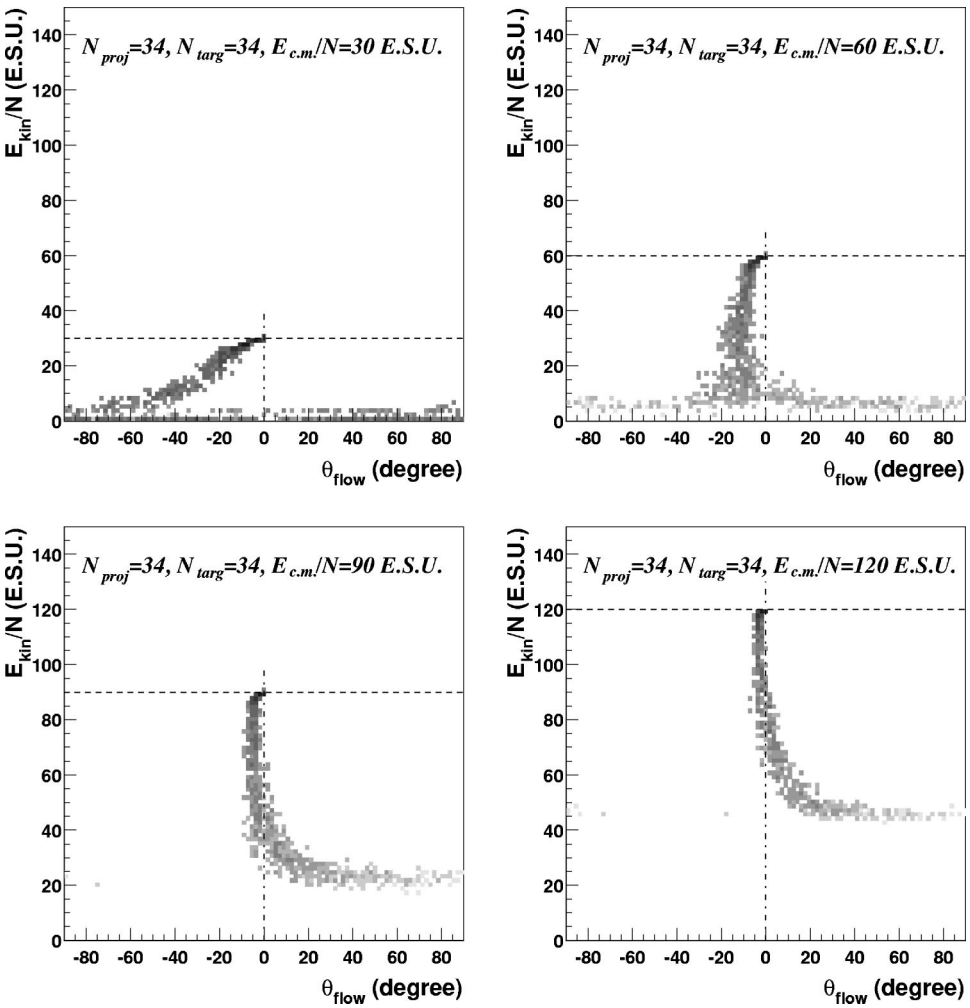

FIG. 10. Wilczinky plots $d^2\sigma/dE_{kin}d\theta_{flow}$ in arbitrary units for $N_{proj}=34$ on $N_{targ}=34$ collisions at different available energies in the center of mass (see text). On each plot, the darkest gray regions correspond to the highest differential cross section values.

$$E^*=\sum_{i=1}^{N} E^i_{kin}+\sum_{i,j>i} V(r_{ij})-E_{Bind}(N), \qquad (4)$$

where E^i_{kin} is the kinetic energy of the particle i in the cluster center of mass frame, r_{ij} the relative distance between the particles i and j, $V(r_{ij})$ the potential energy and $E_{Bind}(N)$ the binding energy of the ground state of the cluster with N particles. This excitation energy is determined at the end of the calculation corresponding to $t=200$ TSU. This energy is very close to that obtained at the separation time of the clusters (the smallest time at which clusters can be identified), since in this time range the evaporation is very weak and the clusters have no time to cool down significantly [22]. On each panel of Fig. 11, the full line corresponds to the expected correlation between E^*/N and $V_\parallel$ for a pure binary scenario (the excitation energy is only due to the velocity damping of each partner), the horizontal dashed line to the energy of the least bound particle for the fused system $N=68$ and the small circle is centered around the expected values of velocity and excitation energy for the fused system.

At $E_{\mathrm{c.m.}}/N=30$ ESU, the points are slightly below the full line. This means that the excitation energy is strongly linked to the velocity damping. The small shift is due to mass transfers between the projectile and the target, and to promptly emitted clusters. The area corresponding to the fused system is well populated showing that a complete fusion process occurs. At $E_{\mathrm{c.m.}}/N=60$ ESU, the distribution of points is roughly compatible with the pure binary process hypothesis except for cluster velocities that lead to excitation energies per particle higher than $E_{LeastBound}$ in the pure binary process picture. For these clusters, E^*/N is always smaller than $E_{LeastBound}$. The complete fusion process area, located above $E_{LeastBound}$, is empty. For the two highest energies, this trend is enhanced. Around the projectile and the target velocity the clusters have an excitation energy compatible with the pure binary process hypothesis. Around the center of mass velocity, when this picture would give excitation energies per particle higher than $E_{LeastBound}$, one finds clusters at small excitation energies. The energy of the least bound particle seems to be a limit to the excitation energy, which can be stored in these clusters.

This can be more clearly seen when the excitation energy E^*/N is plotted as a function of N, as in Fig. 12. On each panel, the full line corresponds to the energy of the least bound particle $E_{LeastBound}$ in the cluster and the dashed line to the binding energy per particle E_{bind}/N. As in Fig. 11, the small circle corresponds to the expected values for the fused system. At $E_{\mathrm{c.m.}}/N=30$ ESU, the area corresponding to complete fusion is filled and all the available energy can be

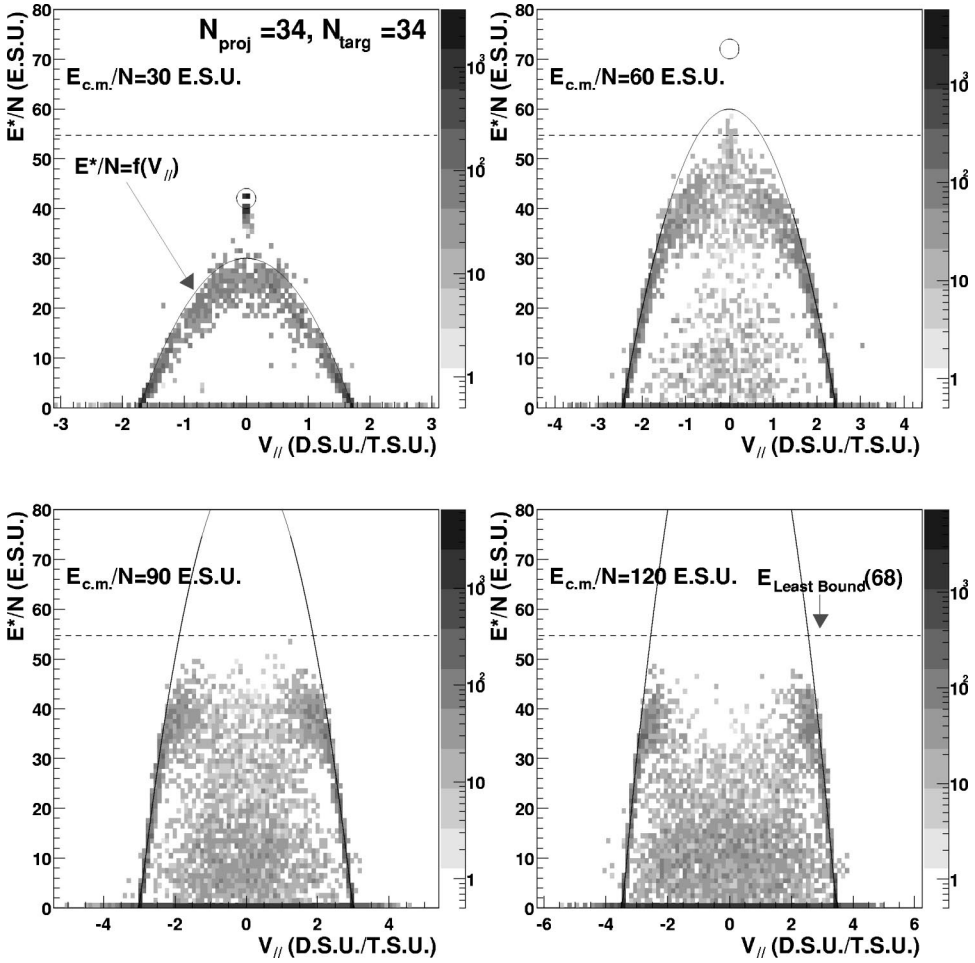

FIG. 11. Excitation energy of clusters versus their parallel velocity $d^2\sigma/d(E^*/N)dV_{\|}$ in arbitrary units for $N_{proj}=34$ on $N_{targ}=34$ collisions at different available energies in the center of mass. On each panel, the full line corresponds to the expected evolution for a pure binary process, the dashed horizontal line corresponds to the energy of the least bound particle for $N=68$, and the circle corresponds to the expected values for the fused system. Different shades of gray indicate different cross sections values as shown on the scales on the right side of each panel.

stored as excitation energy. But for higher energies, one can clearly see that for each fragment size, E^*/N never overcomes $E_{LeastBound}$. At $E_{\mathrm{c.m.}}/N=60$ ESU clusters with sizes higher than the projectile size and the target size can be seen. This area corresponds to an incomplete fusion process. For the two highest energies ($E_{\mathrm{c.m.}}/N=90$ ESU and $E_{\mathrm{c.m.}}/N=120$ ESU), the plots are almost identical: there is no more fusion and the clusters are smaller than the target and than the projectile. One can notice that E^*/N never reaches the binding energy E_{bind}/N except for small clusters where E_{bind}/N and $E_{LeastBound}$ are equal.

This limitation of excitation energy can be understood quite easily. The least bound particle remains bound to the cluster only if its total energy is negative, i.e., its kinetic energy due to the excitation is below its potential one. If one assumes that the excitation energy is roughly equally shared over all particles in the cluster, when the kinetic energy balances the potential energy of the least bound particle, this particle is no more bound to the cluster and can escape. To be observed for a long time, the excited cluster must have an excitation energy per particle below the energy of the least bound particle.

The mechanism of energy deposition in classical N-body clusters seems to be the following one: the excitation seems to be mainly driven by the velocity damping of the two partners and to a lesser extent by exchanges of particles between them. Energy deposition in N-body clusters via cluster-cluster collisions is limited by $E_{LeastBound}$ of clusters. Once the available energy per particle in a cluster is greater than the energy of its least bound particle, unbound particles and/or clusters are rapidly emitted, leaving the remaining cluster with an excitation energy per particle below the energy of its least bound particle. As a consequence, the highest energy deposition per particle can only be obtained at energies close to $E_{LeastBound}$. For higher available energies, the system fragments quickly, leaving rather ''cold'' clusters around the center of mass velocity. Providing this is also true for nucleus-nucleus collisions, this could be an explanation to the quite low excitation energies of fragments found in central collisions of the Xe + Sn system at 50A MeV [30]. This subject will be more completely covered in a forthcoming paper.

C. Statistical description of collisions

Let us end with fragment size analyses of cluster-cluster collisions. In nucleus-nucleus collision studies, such analyses are very often used to fix the parameters of statistical models and to verify the compatibility of statistical decay models with experimental data (see, for example, [31–33]). The so-called Dalitz plots for central ($0\leqslant b/b_{max}<0.1$) $N_{proj}=34$ on $N_{targ}=34$ collisions are shown on Fig. 13. Each panel corresponds to a fixed available energy in the center of mass ranging from $E_{\mathrm{c.m.}}/N=30$ to 120 ESU. For this analysis,

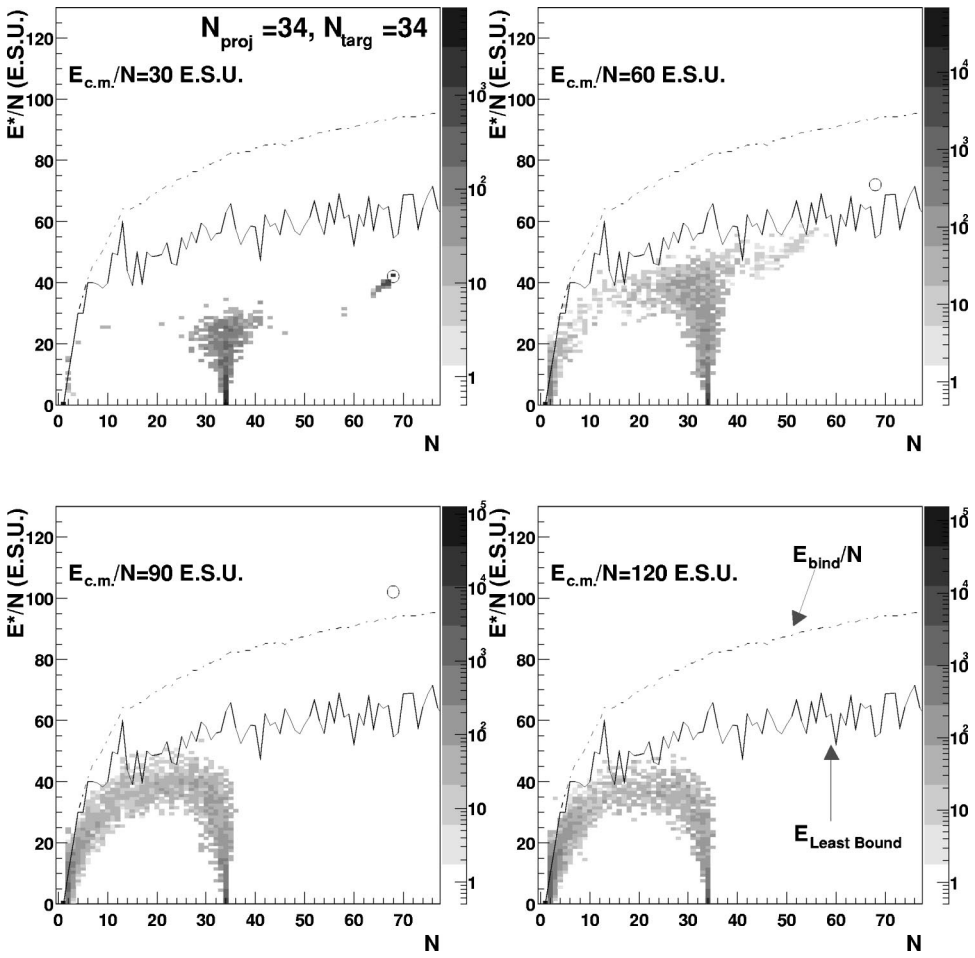

FIG. 12. Excitation energy of clusters versus $N\ d^2\sigma/d(E^*/N)dV_{\parallel}$ in arbitrary units for $N_{proj}=34$ on $N_{targ}=34$ collisions at different available energies in the center of mass. On each panel, the full line corresponds to the energy of the least bound particle, the dashed line corresponds to the binding energy per particle, and the circle corresponds to the expected values for the fused system. Different shades of gray indicate different cross sections values as shown on the scales on the right side of each panel.

only the three heaviest clusters are taken into account. Each event is associated to a point in this plot. The distance of one point with respect to each edge of the triangle is proportional to the size of each of the three clusters. The corners of the triangle correspond to events with one large cluster and two small ones (fusion/evaporation process), an event in the middle of an edge of the triangle corresponds to an event with two equal size clusters and one small one (fission process or binary collision) and the center of the triangle corresponds to three equal size clusters (multifragmentation process). One can see that when the available energy increases, the reaction mechanism goes continuously from fusion/evaporation to binary collisions and finally to multifragmentation and/or vaporization.

This picture is qualitatively very similar to that obtained in SMM calculations [12], describing the decay of a single source, as shown on Fig. 14. In this case, each panel corresponds to an excitation energy. As in Fig. 13, the lowest energies correspond to fusion/evaporationlike processes, with a continuous transition towards fission and multifragmentation when the excitation energy increases.

The strong qualitative similarity between these two pictures suggests that it could be possible to build a statistical decay code that would give the same results as the dynamical simulation. Of particular interest would be the study of the relationship between the parameters of the statistical decay code (size of the source, excitation energy, deformation, radial flow, freeze-out volume, etc.) and the parameters of the dynamical one (projectile and target sizes, impact parameter, bombarding energy, parameters of the two-body interaction). This could also allow to check under which conditions the statistical decay code can be applied. This study could finally allow us to have a consistent description of cluster-cluster collisions, where the parameters of the statistical decay model are deduced from the parameters of the dynamical simulation. In this case, the cluster-cluster collisions could be described completely with a reduced number of parameters.

IV. CONCLUSIONS

As it has been seen in this brief overview of the characteristics and the reaction mechanisms of N classical particles in strong interaction, there are strong qualitative similarities between these systems and the atomic nuclei. The static properties and the reaction mechanisms observed for the atomic nuclei and for these classical clusters are found to be very close to each other. This could mean that the experimental observations made for nucleus-nucleus collisions are mainly governed by the N-body character of the systems and by the overall shape of the two-body interaction (finite range attractive part and short range repulsive part). More physical ingredients (Coulomb interaction, quantum mechanics, mo-

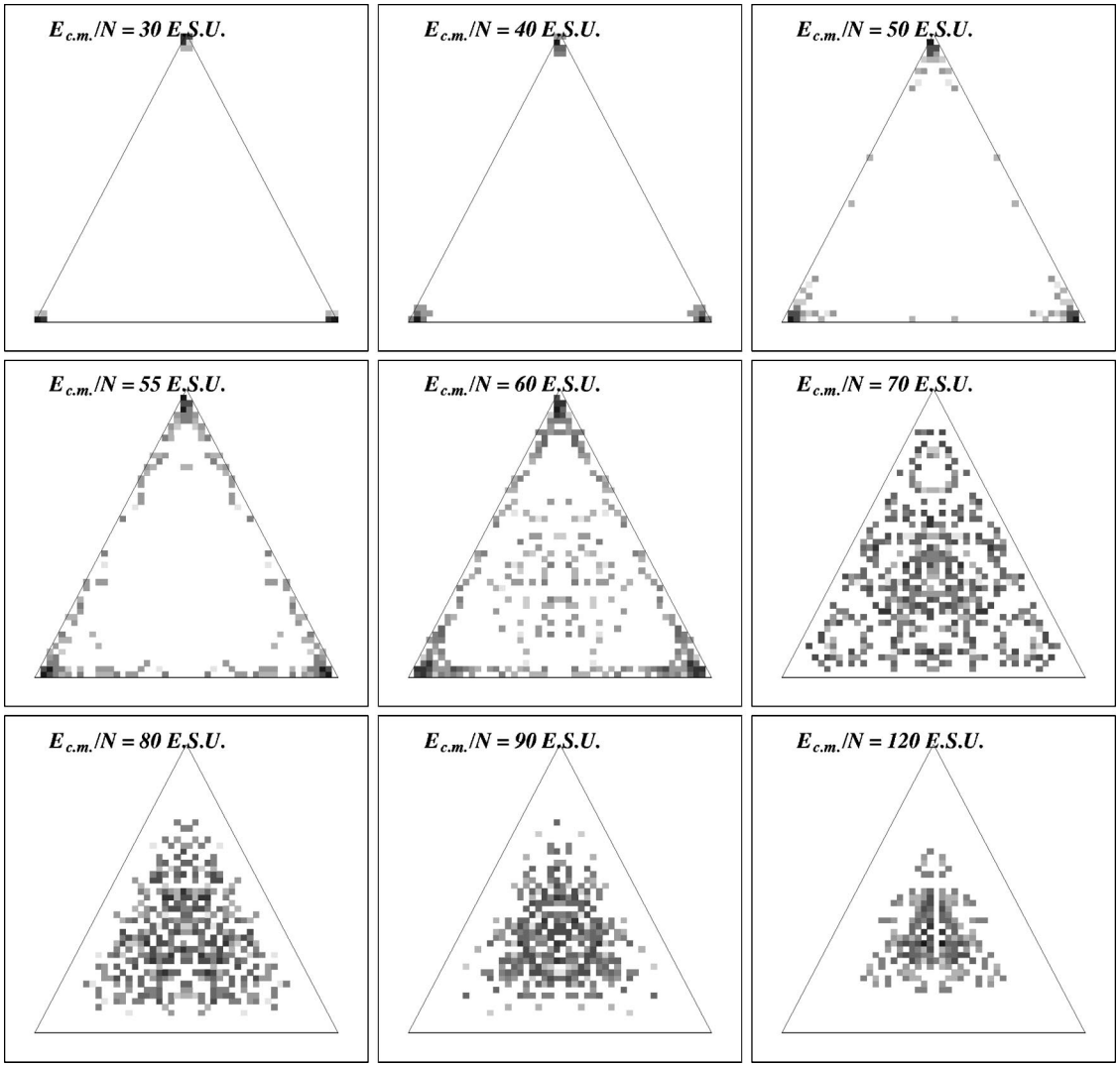

FIG. 13. Dalitz plots for CNBD simulations for central ($0 \leqslant b/b_{max} < 0.1$) $N_{proj} = 34$ on $N_{targ} = 34$ collisions at different available energies in the center of mass. On each plot, the darkest gray region corresponds to the highest cross section value.

mentum dependent interaction) are, of course, necessary if one wants to have a quantitative agreement with experimental data. But it is surprising to achieve such a good qualitative agreement while essential physical ingredients are missing in the simulation.

Since all kinds of reaction mechanisms are observed in these classical simulations, from the low energy fusion/evaporation processes to the high energy participant/spectator processes, they may also allow to connect in a consistent way the mean-field and the nucleon-nucleon approaches. One could, for example, study the relation between the incompressibility modulus and the size of the repulsive part of the interaction (K_∞ and σ_{nn} in the nuclear case). It is well known in transport calculations that one can ''stiffen'' the effective equation of state by just increasing the value of the nucleon-nucleon cross section σ_{nn} [34].

For these classical systems, the energy of the least bound particle $E_{LeastBound}$ seems to play a particular role. For $E_{\mathrm{c.m.}}/N$ below $E_{LeastBound}$ ($\approx$60 ESU), mean-field processes dominate (fusion, deep inelastic and transfer reactions, particles exchange). For $E_{\mathrm{c.m.}}/N$ above $E_{LeastBound}$ the repulsive two-body character of the interaction dominates (promptly emitted particles, participant spectator process, multifragmentation). The energy of the least bound particle of the cluster is also a limit for the energy deposition in the cluster. No scaling between this simulation and nuclear data can be easily made because many ingredients are missing in this model. It is not obvious how the behavior of these classical systems is changed by the inclusion of the Coulomb force, a momentum dependent interaction and quantum mechanics. It would be interesting to check if the energy of the last-populated level in nuclei could play the same role for nuclei as $E_{LeastBound}$ for these classical systems.

Finally, such simulations may reconcile two approaches that were up to now often opposed in nuclear physics: the dynamical description and the statistical description of fragment production. Dynamical models are unique tools to establish the link between the parameters of the interaction and

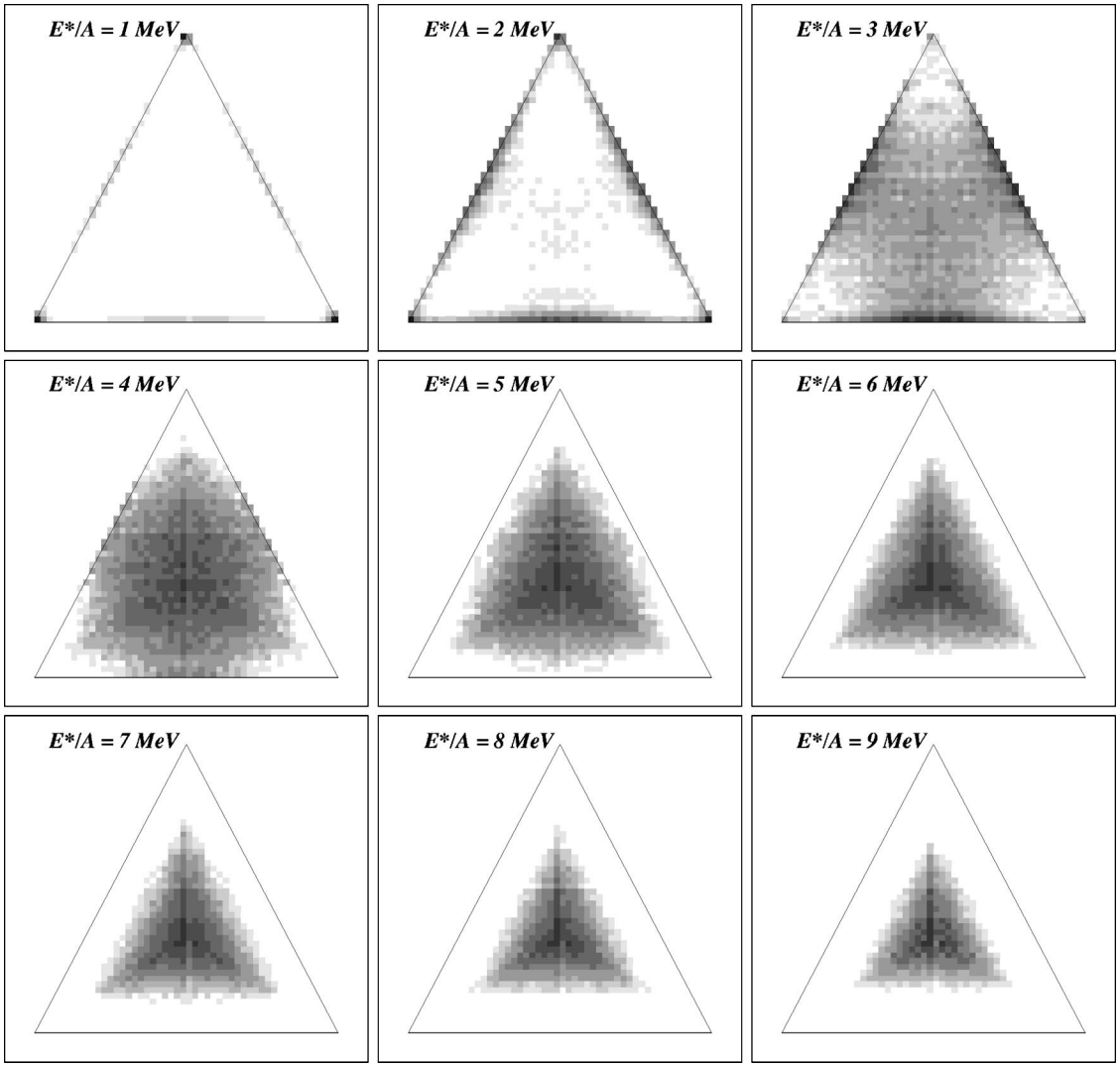

FIG. 14. Dalitz plots obtained with SMM calculations for different excitation energies. The source has a charge $Z=86$, a mass $A=205$, and the freeze-out density is $\rho_{f.o.}=\rho_0/3$. On each plot, the darkest gray region corresponds to the highest cross section value.

those of the statistical models. Additionally, one can determine under which conditions the use of statistical models can be justified, and what are the true meanings of the parameters used in statistical models (temperature, chemical potentials, freeze-out volumes, etc.). This study may allow to have a complete and consistent description of colliding *N*-body systems with a reduced number of free parameters. This could be not only useful for nuclear physics, but also for other fields of physics, for example, cluster physics.

ACKNOWLEDGMENTS

I would like to thank my colleagues of the INDRA Collaboration and from the Laboratoire de Physique Corpusculaire de Caen for a careful reading of this paper. I especially thank Denis Lacroix for suggestions and fruitful discussions, and John Frankland for the corrections of the text. I would also like to thank O. Lopez and A. Botvina for the SMM calculations.

[1] S. E. Koonin, Prog. Part. Nucl. Phys. **4**, 283 (1979).
[2] J. Cugnon *et al.*, Nucl. Phys. **A352**, 505 (1981).
[3] C. Grégoire *et al.*, Nucl. Phys. **A465**, 317 (1987).
[4] A. Bonasera *et al.*, Phys. Rep. **243**, 1 (1994).
[5] G. Bertsch, Phys. Rev. C **29**, 673 (1984).
[6] S. Ayik and C. Grégoire, Nucl. Phys. **A513**, 187 (1990).
[7] J. Aichelin, Phys. Rep. **202**, 233 (1991).
[8] A. Ono *et al.*, Phys. Rev. C **48**, 2946 (1993).
[9] H. Feldmeier, Nucl. Phys. **A428**, 147 (1990).
[10] R. Charity *et al.*, Nucl. Phys. **A511**, 59 (1990).
[11] D. Durand, Nucl. Phys. **A541**, 266 (1992).
[12] J. Bondorf *et al.*, Phys. Rep. **257**, 133 (1995).
[13] D. H. E. Gross, Rep. Prog. Phys. **53**, 605 (1990).
[14] J. Konopka *et al.*, Phys. Rev. C **50**, 2085 (1994).

[15] W. Friedman, Phys. Rev. C **42**, 667 (1990).
[16] T. J. Schlagel and V. R. Pandharipande, Phys. Rev. C **36**, 162 (1987).
[17] C. Dorso and J. Randrup, Phys. Lett. B **215**, 611 (1988).
[18] V. Latora *et al.*, Nucl. Phys. **A572**, 477 (1994).
[19] J. Bondorf *et al.*, Nucl. Phys. **A624**, 706 (1997).
[20] X. Campi, H. Krivine, and N. Sator, Nucl. Phys. **A681**, 458 (2000).
[21] E. Plagnol *et al.*, in Proceedings of the XXXIX International Winter Meeting on Nuclear Physics, 2001, edited by I. Iori.
[22] A. Strachan and C. Dorso, Phys. Rev. C **59**, 285 (1999).
[23] H. Feldmeier and J. Schnack, Rev. Mod. Phys. **72**, 655 (2000).
[24] W. H.Press, B. P. Flannery, S. A. Teukolsky, and W. T. Vetterling, *Numerical Recipes* (Cambridge University Press, Cambridge, 1989).
[25] C. Dorso, S. Duarte, and J. Randrup, Phys. Lett. B **188**, 287 (1987).
[26] D. J. Wales and J. P. K. Doye, J. Phys. Chem. A **101**, 5111 (1997).
[27] J. Wilczynski, Phys. Lett. **47B**, 313 (1973).
[28] C. Dorso and J. Randrup, Phys. Lett. B **301**, 328 (1993).
[29] INDRA Collaboration, V. Métivier *et al.*, Nucl. Phys. **A672**, 357 (2000).
[30] INDRA Collaboration, N. Marie *et al.*, Phys. Rev. C **58**, 256 (1998).
[31] INDRA Collaboration, N. Marie *et al.*, Phys. Lett. B **391**, 15 (1997).
[32] M. D'Agostino *et al.*, Nucl. Phys. **A650**, 329 (1999).
[33] INDRA Collaboration, F. Bocage *et al.*, Nucl. Phys. **A676**, 391 (2000).
[34] V. De La Mota, F. Sébille, M. Farine, B. Remaud, and P. Schuck, Phys. Rev. C **46**, 677 (1992).